REGULARIZED ESTIMATION OF FLOW PATTERNS IN MR VELOCIMETRY.

A. Herment, J.-F. Giovannelli, E. Mousseaux, J. Idier*, A. Decesare, O. Jolivet and J. Bittoun.*

INSERM U.66 CHU Pitié 91 Bld. de l'Hôpital, 75013 Paris France
*LSS - Supélec - UPS Plateau de Moulon, 91192 Gif sur Yvette Cedex, France

ABSTRACT

A Bayesian estimator of the magnetic resonance (MR) velocity image is proposed. It is based on a Markov model accounting for the spatial structure of the flow velocity. On the other hand, low MR signal intensity yields high uncertainty on the velocity. Such an important property is taken into account through the observation model. The resulting posterior likelihood is optimized using an Iterative Coordinate Descent (ICD) algorithm. Compared to the usual least squares solution, simulation results on flows with parabolic and flat profiles demonstrate a significant gain of in the mean square error.

1. INTRODUCTION

MR velocity imaging is based on the dependence of the MR signal phase on the flow intensity. More precisely, the phase of the signal is related to the velocity component in the direction of a bipolar velocity phase-encoding gradient. Therefore, a velocity image can be built, voxel by voxel, from the phase differences or from the mean frequency of the MR signal recorded in each voxel using linearly increasing velocity encoding gradients [1]. Different methods have been proposed to improve intra-voxel precision and noise robustness of MR velocimetry. Such methods are usually based on weighted least squares [2] and on zero padded Fourier transformation [3]. To conciliate both short acquisition time and robust velocity estimation, we propose a new regularized approach to velocity imaging.

2. REGULARIZED VELOCITY ESTIMATION

2.1. Basics for regularization

The proposed method relies on the hypothesis of a coherent organisation of flows.

(H_1) Viscosity forces in blood impose a spatial correlation of the velocities between adjacent voxels.

As a consequence, independent processing of data for each voxel is clearly suboptimal. Other specificities of MR flow signals should also be taken into account.

(H_2) The time of flight effect increases MR signal magnitude in the flowing blood regions due to the incoming of new unsaturated spins in the analysed section. In other words, strong MR signals provide a higher reliability in terms of velocity measurement.

(H_3) MR signals in tissues surrounding the vessels can either be weak such as in the lung, or high as in the liver. In the first case, the raw data provide poor velocity information, whereas it is well contrasted in the second case.

Estimating the regularized velocity consists of processing the raw MR data set, $\boldsymbol{w}$, composed of N_g complex valued images of $N_x \times N_y$ pixels $\boldsymbol{w}_{g,yx}$.

First, an observation model is constructed for the MR data. Second a likelihood function is built from this model. Third regularization is introduced to obtain the posterior likelihood. Fourth, the solution is reached using a suited optimization method.

0-7803-3258-X/96/$5.00 © 1996 IEEE

2.2. Modelization

The classical assumption of a uniform velocity inside each voxel and the general strategy given in the introduction for gradient encoding [3] indicate that, in a given voxel, the velocity information is coded as the frequency v_{yx} of a complex exponential:

$$z_{yx} = \left[1,\ e^{-2i\pi v_{yx}},\ e^{-4i\pi v_{yx}},\ \ldots.\ e^{-2N_g i\pi v_{yx}}\right]^t \quad (1)$$

with a magnitude a_{yx}. An additive Gaussian noise accounts for electronic noise in the reception antenna and also models errors. The resulting observation model reads:

$$\boldsymbol{w}_{yx} = a_{yx}\, z_{yx} + \boldsymbol{b}_{yx} \quad (2)$$

For sake of simplicity, spatial decorrelation is assumed and each $\boldsymbol{b}_{yx}$ is considered as a zero-mean stationary white Gaussian vector with variance r_b.

2.3. Definition of the likelihood

Let $\boldsymbol{a}$ and $\boldsymbol{v}$ denote the vectors of magnitudes a_{yx} and frequencies v_{yx} respectively. Eq. (2) and the structure of noise yield the following likelihood:

$$f(\boldsymbol{w} \mid \boldsymbol{a}, \boldsymbol{v}) = \prod_{xy} f(w_{yx} \mid a_{yx} z_{yx})$$
$$\propto \exp -\frac{1}{r_b} \sum_{yx} (w_{yx} - a_{yx} z_{yx})^t (w_{yx} - a_{yx} z_{yx}) \quad (3)$$

2.4. Priors on $\boldsymbol{a}$ and $\boldsymbol{v}$

For sake of simplicity, no statistical dependence is introduced in the prior model between $\boldsymbol{a}$ and $\boldsymbol{v}$, so that:

$$f(\boldsymbol{a},\boldsymbol{v}) = f(\boldsymbol{a})\, f(\boldsymbol{v}) \quad (4)$$

– Prior model for $\boldsymbol{a}$

Since our study is focused on the velocity field, no prior knowledge of a spatial structure for $\boldsymbol{a}$ is introduced. It is simply assumed to be a white zero-mean Gaussian vector with variance r_a:

$$f(\boldsymbol{a}) = \prod_{xy} f(a_{yx}) \propto \exp \frac{-1}{r_a} \sum_{yx} a^*_{yx} a_{yx} \quad (5)$$

– Prior model for $\boldsymbol{v}$

In order to account for spatial coherence of the flow (H_1), prior model for $\boldsymbol{v}$ is chosen as a first order Markov field:

$$\log f(\boldsymbol{v}) \# -\lambda\varphi_1(\boldsymbol{v}) - \mu\varphi_2(\boldsymbol{v}), \quad (6)$$

$$\varphi_1(\boldsymbol{v}) = \sum_{xy} \varphi\left(v_{y,x+1} - v_{y,x}\right) + \varphi\left(v_{y+1,x} - v_{y,x}\right) \quad (7)$$

and

$$\varphi_2 = \sum_{xy} \varphi\left(v_{yx}\right) \quad (8)$$

where:

$$\varphi(u) = 2\alpha\sqrt{\alpha^2 + u^2} - 2\alpha^2 \quad (9)$$

An edge-preserving L_1-L_2 norm $\varphi(u)$ has been chosen, so that $\varphi_1(u)$ introduces locally smooth spatial structures, while it still allows abrupt spatial changes of velocity, for instance at the boundaries of flat profiled flows. On the other hand, the second term $\varphi_2(u)$ incorporates the same norm to draw low velocities towards zero in agreement with assumption (H_3) in surrounding tissues.

2.5. Posterior density

Fusion of the likelihood and prior is achieved by the Bayes' rule. The posterior density reads:

$$f(\boldsymbol{a}, \boldsymbol{v} \mid \boldsymbol{w}) \propto f(\boldsymbol{w} \mid \boldsymbol{a}, \boldsymbol{v})\, f(\boldsymbol{a})\, f(\boldsymbol{v}) \quad (10)$$

Maximum a posteriori (MAP) estimation corresponds to the minimization of the following criterion:

$$Q(\boldsymbol{a}, \boldsymbol{v}) = \sum_{xy} \left[\frac{1}{r_b} \left\| \boldsymbol{w}_{yx} - a_{yx} z_{yx} \right\|^2 + \frac{1}{r_a} \left| a_{yx} \right|^2 \right] \quad (11)$$
$$+\lambda\varphi_1(\boldsymbol{v}) + \mu\varphi_2(\boldsymbol{v})$$

2.6. Optimization with respect to $\boldsymbol{a}$

Since the criterion is quadratic with respect to $\boldsymbol{a}$, explicit minimization is possible. Moreover the MAP estimate of $\boldsymbol{a}$ does not depend on $\boldsymbol{v}$:

$$\hat{a}_{yx} = (1 + \frac{r_b}{r_a})\, FT_{w_{yx}}(v_{yx}) \quad (12)$$

where $FT_{w_{yx}}(\nu_{yx})$ stands for the Fourier transform of w_{yx}. The resulting partially optimized criterion becomes a function of v only:

$$Q(v) = -\frac{N_g^2}{r_a}\left(1+\frac{r_b}{r_a}\right)^2 \sum_{xy} P_{w_{yx}}(\nu_{yx}) \qquad (13)$$

$$+\lambda\varphi_1(v)+\mu\varphi_2(v)$$

where $P_{w_{yx}}(\nu_{yx})$ is the periodogram of w_{yx}. Note that expression (4) naturally accounts for assumption (H_2), since each vector of data w_{yx} enters the criterion in proportion to its empirical energy.

2.7. Optimization with respect to v

Minimization of criterion (4) is not an easy task because the periodograms $P_{w_{yx}}(\nu_{yx})$ are not necessarily well-behaved. We propose an Iterative Coordinate Descent (ICD) to perform suboptimal minimization. The criterion is successively and iteratively minimized with respect to each ν_{yx}, so that the criterion is guaranteed to decrease at each iteration. According to our experience, this technique is much more suited here than a gradient approach, which would be easily trapped in the local minima induced by the shape of the periodograms.

Initialization is performed by taking the maximum of each periodogram in the base frequency band. Note that this initial solution would correspond to the true solution without regularization.

3. RESULTS

Synthetic images were created for flows with parabolic and flat profiles together with simulated surrounding tissues with both low and high MR signal magnitude. Figures 1.A and 1.C present the reference flow images used for generating the MR data. A series of four data is assumed available for each pixel ($N_g = 4$), and the SNR is 10 dB. A gray colormap was used, with the zero velocity coded in mid-gray. The low velocity region around the flow simulates (upper right) surrounding tissues in which the MR signal is very low (1%), or with a high (100%) MR signal (lower left). Finally the highest values of the MR signal are encountered inside the flow (100% to 150%).

The velocity images 1.B and 1.E have been calculated using the plain maxima of the periodogram. The well known characteristics of MR velocimetry appear in the velocity images. Some spurious pixels are present. Those found in the flat profiled flow are due to the ambiguity around the Nyquist limit, which cannot be raised from noisy data only. On the other hand, those in the upper right corner correspond to low MR signals.

Figures 1.C and 1.F show the regularized velocity images. Enhancement is clearly visible compared to images 1.B and 1.E. The effect on noise reduction is predominant in surrounding tissues, but the estimated velocities are also more precise inside flow regions. Moreover, the ambiguity around the Nyquist limit is raised thanks to the prior spatial structure.

We have compared the mean square error (MSE) between the estimated images and the reference images. The improvement brought by the regularized approach is close to a factor 900 for parabolic flow and close to 200 for the flat profiled flow.

CONCLUSION

Regularization of velocity patterns obtained in MR velocimetry is possible based on the assumption of a regular flow organization together with using the relationship between reliability of flow information and the intensity of the MR signal. Application of this concept to in-vivo blood flow still needs to address the validity of these hypothesis in strongly pathological turbulent flows.

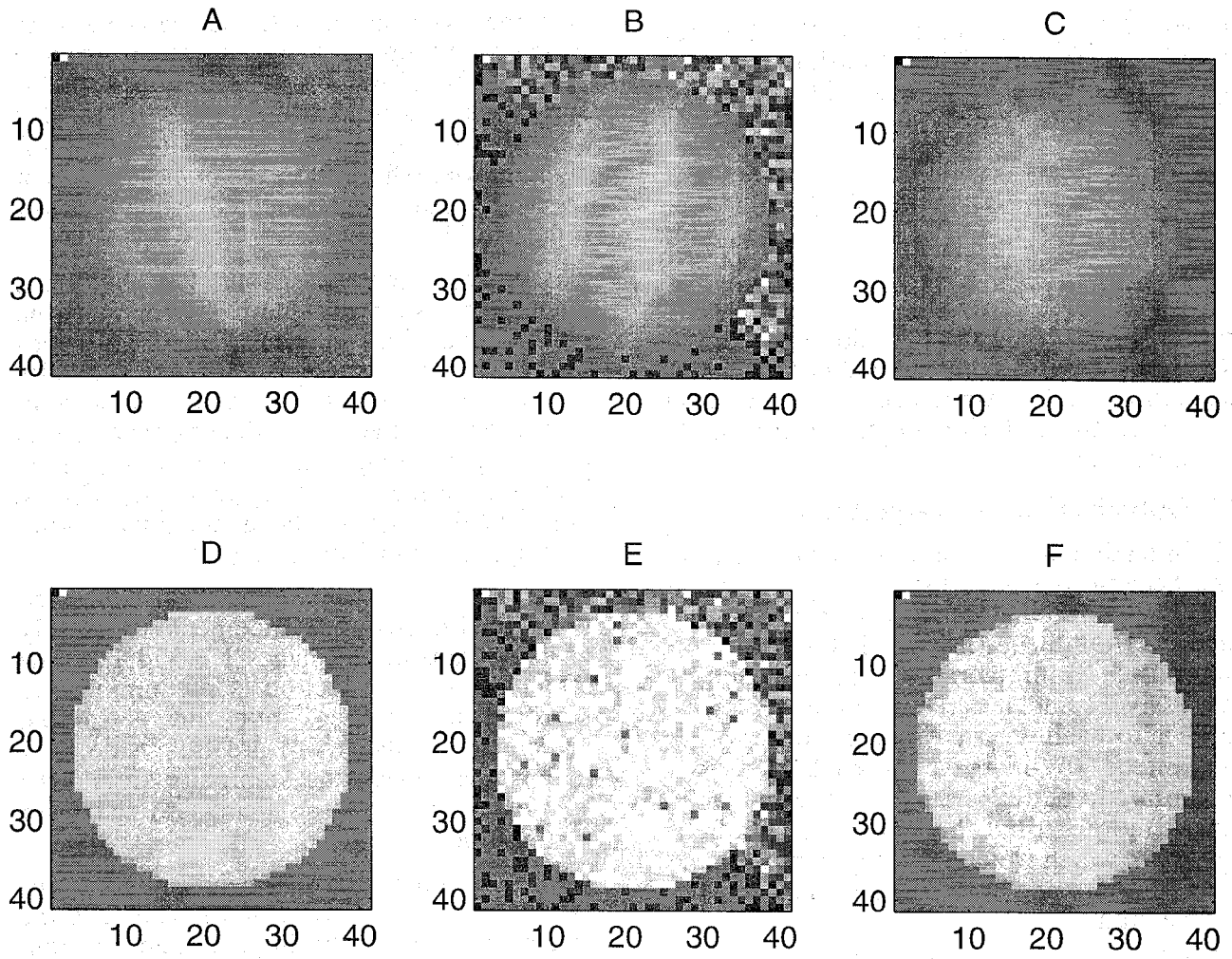

Fig. 2. MR velocity images : Parabolic flow profile. A) Reference image; B) Velocity image; C) Regularized velocity image (μ = 100, λ = 1000). Flat flow profile. D) Reference image; E) Velocity image; F) Regularized velocity image(μ = 400, λ = 600, $\alpha_\lambda = \alpha_\mu = 0.02$).

REFERENCES

[1] G.L. Nayler, D.N. Firmin , D.B. Longmore *et al.*, "Blood flow imaging by cine magnetic resonance", *J. Comput. Assist. Tomog.* 10:715-722, 1986.

[2] A. Caprihan and M.V. Icenogle. "A weighted Least-Squares Method for Nuclear Magnetic Resonance Velocity Imaging", NMR 29:512-520, 1993.

[3] J. Bittoun, E. Bourroul, O. Jolivet *et al.*, "High-precision MR velocity mapping by 3D-Fourier phase encoding with a small number of encoding steps", *J. Magn. Reson.*; 29:674-680, 1993.

Aknowledgments : This work was partially supported by a grant from the "Fondation pour la recherche Medicale".